CHAPTER – 3

Studies on dielectric and magnetic properties of $CaCu_3Ti_3MnO_{12}$ ceramic synthesized via semi-wet route

3.1. Introduction

$ACu_3Ti_4O_{12}$ (Where A= $Y_{2/3}$, $Bi_{2/3}$, $Gd_{2/3}$) type of perovskite oxide was discovered in 1967 [1] which have ability to produce high dielectric constant. From last decade, Scientists across the globe have been using $BaTiO_3$, $Pb(Mg_{1/3}Nb_{2/3})O_3$(PMN), $Pb(Zn_{1/3}Nb_{2/3})O_3$(PZN) as a relaxer ferroelectric which possess high permittivity constant ($\varepsilon r \approx 10^2 – 2\times10^4$) [2]. The main problems with BaTiO3 is ferroelectric in nature i.e. it shows phase transition with increasing temperature and the dielectric constant vary with increasing temperature which made it a bad candidate for ideal capacitor material. Due to these drawbacks, Subramanian et al discovered firstly $CaCu_3Ti_4O_{12}$ (CCTO) complex perovskite oxide with high dielectric constant which is greatly utilized from last two decades for analogous study [3, 4]. Scientists' have reported that the microstructure and impedance properties of CCTO ceramic which greatly influenced by the synthesis route [5, 6].The complex perovskite type of CCTO material shows wide applications in potential affect in ceramic capacitor, dynamic random-access memory, transducers, microelectronic, microwave devices and in other electronic equipment due to its high thermally stability and giant permittivity (10^4-10^5) in temperature range 100-600 K without any structural phase transition [7, 8, 12]. CCTO based ceramic have body centred cubic structure with lattice parameter of 7.391 A^o and space group Im3 [9, 10].Usually, high dielectric constant value is displayed by ferroelectric substances and these are connected to atomic displacement with non-centro symmetrical shape [3].The permittivity and magnetic properties of CCTO ceramic were improved by the doping of different cationic substituents at Cu and Ti-site in $CaCu_3Ti_4O_{12}$ [11].The giant dielectric constant of

CCTO ceramic was widely explained by grain boundary barrier layer (GBBL) capacitors models on the grain boundaries between semiconducting grains [12]. CCTO ceramic studies by impedance spectroscopy reveals that it is heterogeneous in nature containing semiconducting grains and insulating grain boundaries [13, 14]. The activation energy of CCTO was found to be around 0.1 eV [13]. It is reported that high permittivity value of CCTO ceramic is not intrinsic but due to extrinsic which related to their microstructure [15]. Some modifications have been applied for the upgrade of dielectric properties of CCTO ceramic. Since last few years currently well-known process is partial substitution on Cu and Ti site which refine the permittivity and give assistance to understand the genesis of high permittivity response in CCTO ceramic [16, 17]. The dielectric response was also affected by the shape of grains and grain boundaries [18, 19]. Mn-doped CCTO significantly decreases the grain boundaries resistance, permittivity and dielectric loss of CCTO ceramic due to decrease in the grains size for increasing the density on grains boundaries [20, 21]. In this work, we have synthesized the CCTMO through semi-wet route and reported their magnetic, dielectric properties and their microstructures. This procedure has advantage to upgrade permittivity, dielectric loss and magnetic response of CCTMO ceramic.

3.2. Experimental

3.2.1. Synthesis

CCTMO was synthesized through semi-wet route. In this method, chemicals calcium nitrate, $Ca(No_3)_2.4H_2O$ (98% Merck, India), Copper nitrate, $Cu(No_3)_2.3H_2O$ (99% Merck, India),

Manganese acetate, $Mn(CH_3COO)_2.4H_2O$ (99% Merck, India), and titanium oxide, TiO_2 (99% Merck, India), were taken in stochiometric amount in molar ratio. Solution of $Ca(No_3)_2.4H_2O$, $Cu(No_3)_2.3H_2O$, and $Mn(CH_3COO)_2.4H_2O$ were prepared in distilled water. All the solutions were mixed together in beaker and stochiometric amount of solid TiO_2 was added in solution. Calculated amount of citric acid (99.5%, Merck India) equivalent to metal ions was dissolved in distilled water and mixed with the solution. The resulting solution was heated on a hot plate magnetic stirrer at 343-353 K to evaporate water and allows for self-ignition. A fluffy mass of CCTMO powders was obtained after removal of a lot of gases. Citric acid used as a complexing agent that acts as fuel in ignition step. The resulting CCTMO powder was ground with the help of agate and mortar to make fine powder. The Powder was calcined at 1123 K for 6 h. Calcined powder was used to make for cylindrical pellets with the using of 2% PVA as a binder on applying 5 tons of pressure using hydraulic pressure for 90 second. Finally, the CCTMO pellets were sintered at 1223 K for 8 h.

3.2.2. Characterization

Thermogravimetric analysis (TGA) of CCTMO powder was used in the air at the heating rate 10^0C/ minute from room temperature to 1073 K using with the help of thermal analyser (PerkinElmer, USA). The crystalline phase of CCTMO ceramic sintered sample was identified by X-ray diffractometer (Rigaku miniflex 600, Japan) applying Cu-kα radiation with wavelength 1.5418 A^0. The microstructure and elemental composition were examined by scanning electron microscope (ZEISS; model EVO18 research, Germany) attached with energy-dispersive X-ray (EDX) analyser (Oxford instrument, USA).

The particle size was examined by high resolution transmission electron microscope (HR-TEM, Technai G2 20 S-Twin). For HR-TEM characterization, the samples were dispersed in acetone and sonicated 3 h. This suspension was deposited on carbon coated copper grid and dried in oven 2 h. The thickness and surface morphology were analysed by using Atomic force microscopy (NTEGRA Prima, Germany). The magnetic property of CCTMO was determined by Quantum Design MPMS-3, over a temperature range 5 to 300 K at magnetic field ± 2 T. Temperature difference of zero field cooled (ZFC) were determined at 100 Oe applied field were carried out using SQUID VSM dc magnetometer. The dielectric data of silver coated cylindrical pellets were examined by LCR meter (PSM1735, NumetriQN_4L, and U.K.).

3.3. Results and discussion

3.3.1. X-ray diffraction studies

Figure 3.1 shows the X-ray Diffraction pattern of CCTMO ceramics sintered at 1223 K for 8 h. The entire diffraction pattern is correctly matched with the JCPDS (card no.21-0140), confirmed the single-phase formation of CCTMO ceramic having body cantered cubic structure along with the minor secondary phase JCPDS (card no.46-1238) of TiO_2 [22].

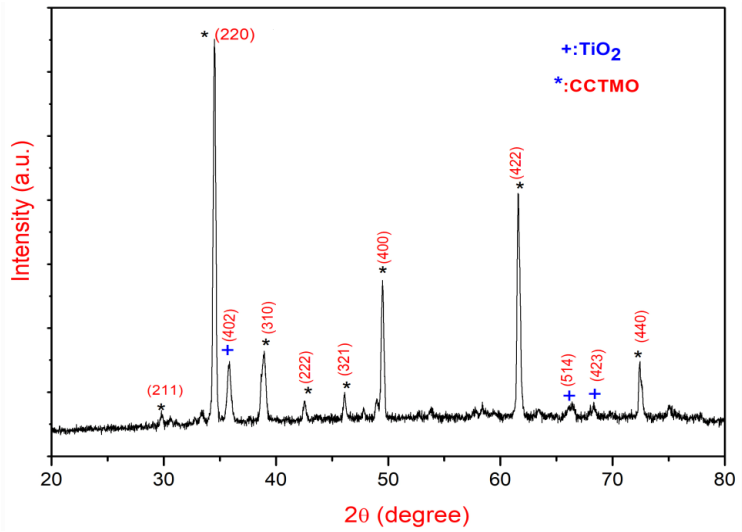

Fig. 3.1 XRD diffraction pattern of sintered CCTMO at 1223K for 8 h.

The crystalline size (D) of CCTMO was calculated by using Debye Scherrer formula.

$$D = \frac{K\lambda}{\beta COS\theta} \quad (1)$$

where D is crystallite size, k is constant equal to 0.89, λ is wavelength of X-ray, θ is the Bragg diffraction angle and β is the full width at half maximum (FWHM) in radians. For the calculation of correct value of crystallite size, the line broadening due to instrument effect eliminated by using standard sample for XRD data. The average crystalline size of CCTMO calculated from XRD data are 34.77 ± 10 nm.

3.3.2. Microstructural studies

Figure 3.2 a Shows bright field TEM image of CCTMO ceramic sintered at 1223 K for 8 h reveals the nanocrystalline nature of the particles. The observed particle size calculated by TEM measurement is found to be 43.76 ± 10 nm. The

particle size observe from TEM is closed to the average crystallite size which observed by XRD result. The nanocrystalline nature of CCTMO is also confirmed by selected area diffraction (SAED) patterns, shown in Fig. 3.2 (b). The zone axis [U V W] obtained by selected area diffraction (SAED) patterns in between the planes (2 2 1) and (1 1 0) is [$\overline{1}1$ 0], shown in Fig. 3.2 b.

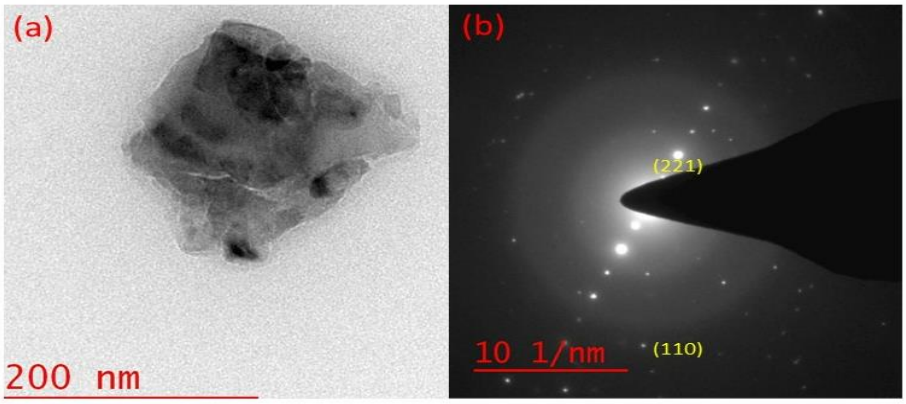

Fig. 3.2 (a) Bright field TEM images (b) Selected area diffraction pattern (SEAD) of CCTMO ceramics sintered at 1223K at 8h.

The SEM micrograph of sintered pellet of CCTMO shows in Fig. 3.3a. Reveals the clear bimodal spherical grain formation with the size of 1.46 µm [23]. It is clear from SEM micrograph smaller grains observed in nanometre and bigger grain in micrometre range [24].The elemental composition of CCTMO observed by using electron diffraction X-ray (EDX) spectroscopy is shown in Fig. 3.3b. The atomic percentage and weight percentage of Ca, Cu, Ti, Mn, and O are found to be 5.62, 14.20, 18.78, 6.67, 54.73 and 6.89, 27.61, 27.52, 11.20, 27.78, respectively. The weight percentage and atomic percentage of CCTMO ceramic confirmed the stochiometric and the purity of the material.

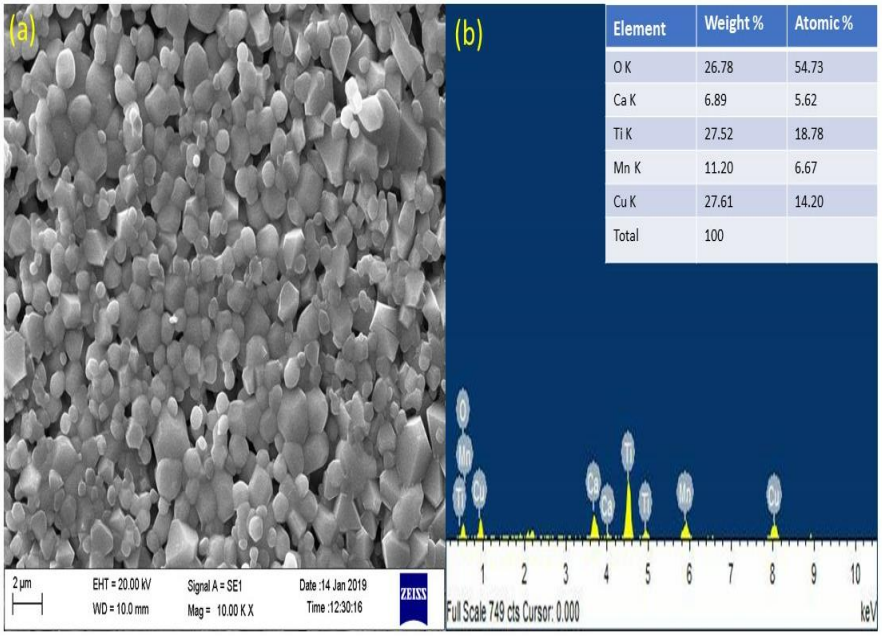

Fig. 3.3 SEM images of CCTMO ceramics sintered at 1223K for 8h, (a) SEM images of CCTMO (b) EDX spectra of CCTMO ceramic.

Figure 3.4a shows 2-D AFM images of CCTMO ceramic sintered at 1223 K for 8 h explains cubical structure of grains which is separated by grain boundary. The average roughness (R_a) and root mean square roughness (R_q) are found to be 0.109 µm and 0.141 µm, respectively on scanned area 40 µm × 40 µm. Fig. 3.4b exhibits the distribution of particle on the surface was examined in 3-D structure. The average roughness (R_a) and root mean square roughness (R_q) are found to be 0.163 µm and 0.209 µm, respectively. The maximum peak-valley depth of two-dimensional structure is to be found 0.40 µm. The grain size obtained by the histogram plots are lie in 1-1.6 µm range and average particle size is found to be 0.3µm out of 513 grains is shown in Fig. 3.4c [25].

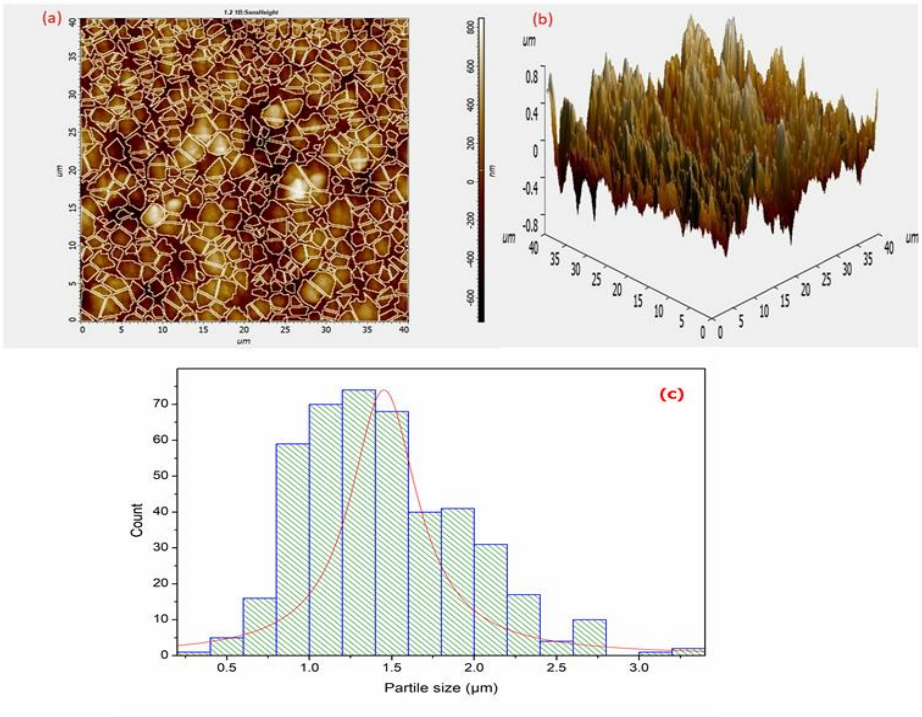

Fig. 3.4 AFM images of CCTMO ceramics sintered at 1223 K for 8 h, (a) 2-dimentional structure (b) 3-dimenional structure (c) bar diagram of particle size.

3.3.3. Dielectric studies

Figure 3.5a Shows temperature dependent dielectric constant at few selected frequencies (1 Hz, 10 kHz, and 100 kHz). It is observed from figure that the dielectric constant of CCTMO almost temperature independent from 300 K to 500 K at all measured frequency on substitution Mn in CCTO ceramic [29].The constant value of ε_r with temperature is observed due to phase transition from ferroelectric to paraelectric. The value of dielectric constant (ε_r) for CCTMO is found to 50 at 1 kHz. Fig. 3.5b shows the variation of dielectric loss (tan δ) with temperature at few selected frequencies. It is clear from figure that tan δ firstly increases from 300 K and decreases after 390 K. The value of tan δ of CCTMO is found to be less than0.233 at all measured frequencies.

Fig. 3.6 (a & b) shows frequency dependent permittivity (ε_r) and dielectric loss tangent (tan δ) at few selected temperatures of CCTMO ceramic. Figure 3.6a shows the permittivity (ε_r) result of CCTMO sample 100 Hz to 1 MHz data indicate that Mn-doping CCTO shows low value of permittivity (10^2 at 1 MHz).The decreasing behaviour of dielectric constant explained by Maxwell-Wagner phenomenon [26]. The dielectric constant was found less than 100 at all measured temperature. The low value of dielectric constant of CCTMO ceramic is due to low conductivity nature of Mn-doped CCTO ceramic. The result indicates that Mn^{4+} partially substituted in place of Ti^{4+} site of CCTO and represented as $CaCu_3Ti_3MnO_{12}$ ceramic shows significant effect in dialectical nature of CCTO [27, 28]. The Mn^{4+} ions enter in to both grain and grain boundary, this response is responsible for significant changes in electrical properties of grains and grain boundaries with increasing the Mn^{4+} ion concentration [27, 28]. Fig. 3.6b shows the variation of dielectric loss (tan δ) from 100 Hz to 1 MHz at few selected temperatures. The value of tan δ of CCTMO was found to be less than0.1 at all selected temperatures.

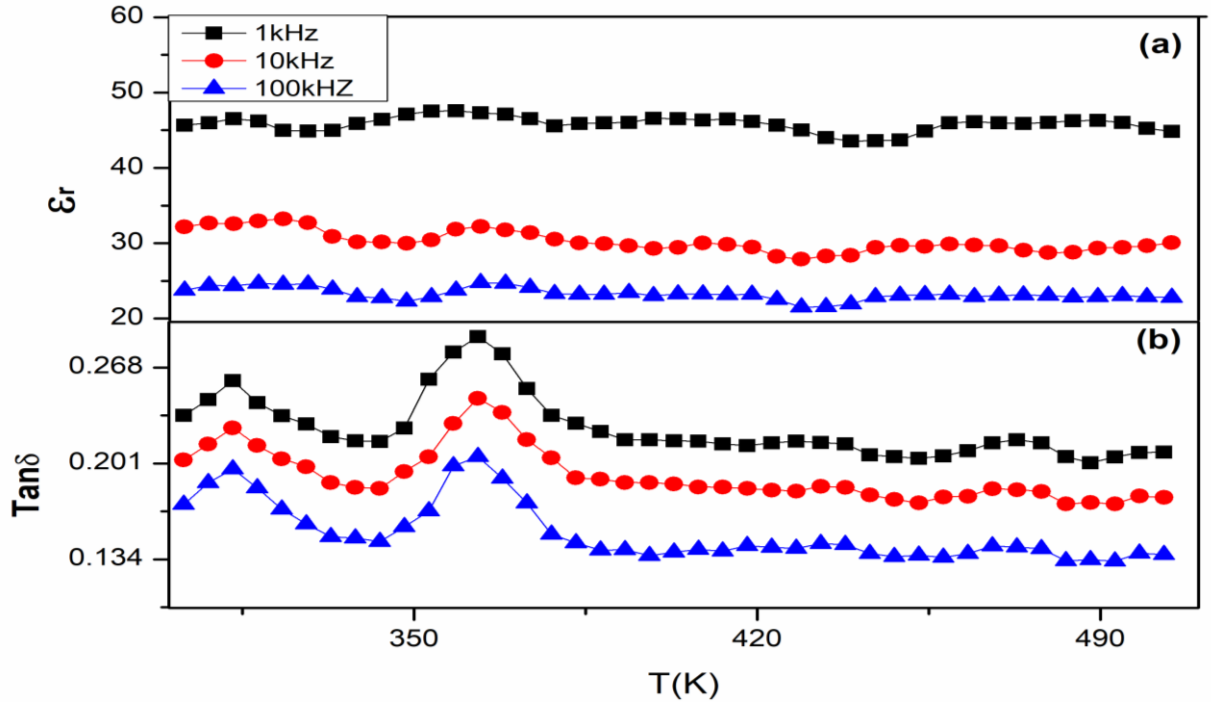

Fig. 3.5 Temperature dependent (a) dielectric constant (ε_r), and (b) dielectric loss (tan δ) at few selected frequencies.

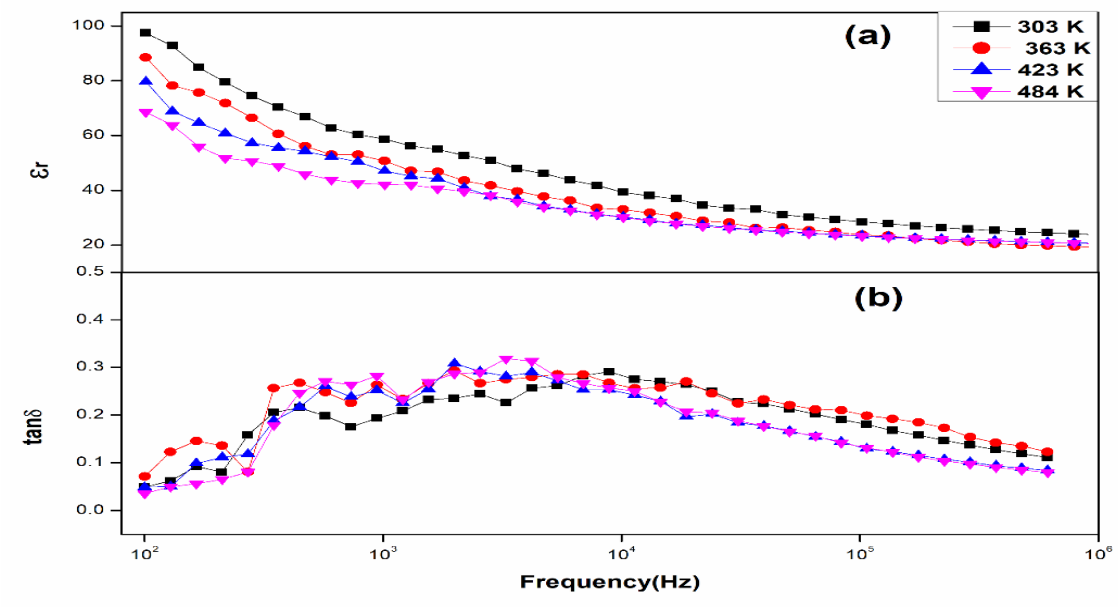

Fig. 3.6 Frequency dependent (a) dielectric constant (ε_r) and (b) Dielectric loss (tan δ) at few selected Temperature.

3.3.4 Magnetic studies

Figure 3.7a depicts the dependence of magnetization of zero field cooled (ZFC) and field cooled (FC) at the temperature is 5 K to 300 K and applied magnetic field is 100 Oe. The compound shows the transition between ferromagnetic to paramagnetic in nature [30].The M-T plots (fig. 3.7a) shows the divergence between ZFC and FC approximately at 30 K. The magnetic behaviour increases rapidly in the FC curve which confirms that the presence of ferromagnetic property in Mn-doped CCTO [31]. However, Mn-doped ZFC and FC curve decrease with increasing temperature. Both ZFC and FC plots shows the two different branches which are merged in to a tail at the Curie temperature. The Curie temperature for Mn-doped CCTO is found to be 94.37 K. The variation of magnetization (M) with magnetic field (H) at two different temperatures (5, 300 K) and applied magnetic field ± 2 T for CCTMO is shown in Fig. 3.7b. M-H hysteresis curves at 5 K temperature explains the ferromagnetic nature and the linear variation in magnetic moment with respect to magnetic field is observed with increase of temperature (300 K) which confirms the presence of paramagnetic nature of the material. The value of magnetic saturation (M_s), remnant magnetisation (M_r) and coercivity (H_c) at lower temperature (5 K) are calculated and found to be 14.09, 9.93 emu/g and +507.088 Oe, respectively [29].

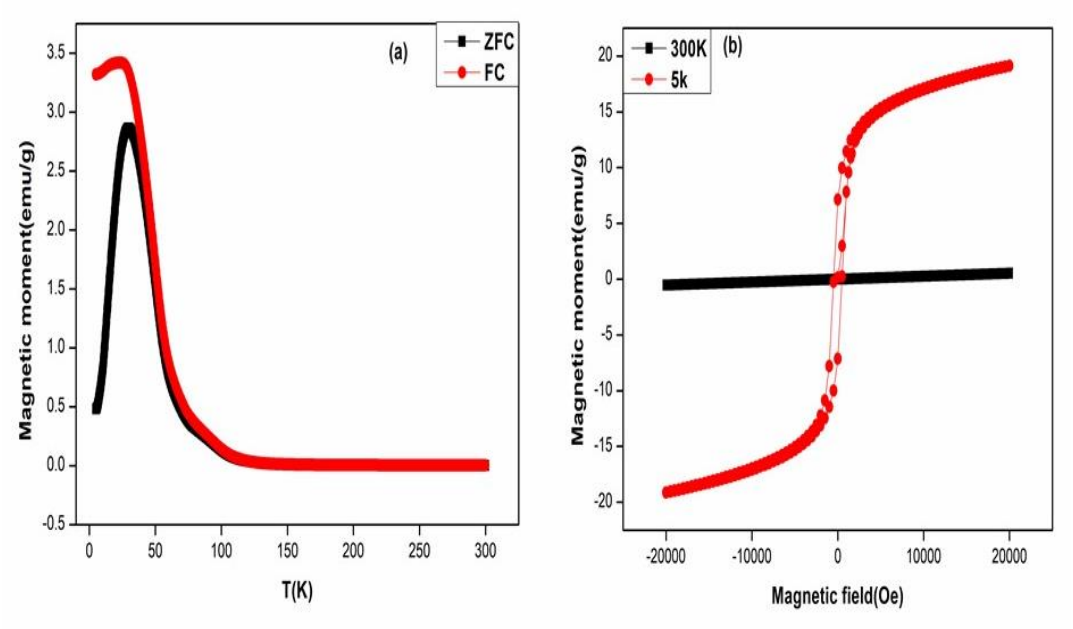

Fig. 3.7 Temperature dependent (a) magnetic moment noted at ± 2 T and magnetic field at 100 Oe. (b) M-H hysteresis at 5 and 300 K for CCTMO ceramic.

Figure 3.8 depicts the temperature dependent reciprocal of magnetic susceptibility for CCTMO ceramic. The Weiss temperature (θ) and Curie constant (C) can be determined by using fitting of the curve with the help of the Curie–Weiss law, represented by fallowing equation.

$$\chi = \frac{C}{T-\theta} \qquad (2)$$

Where, χ is magnetic susceptibility, C is curie constant, θ is Curie Weiss temperature and T is temperature. The calculated value of Curie constant and Weiss temperature obtained by this plot were found to be 220.6 emu/g^{-1} and 94.37 K, respectively. The positive value of θ indicates the ferromagnetic nature of CCTMO ceramic.

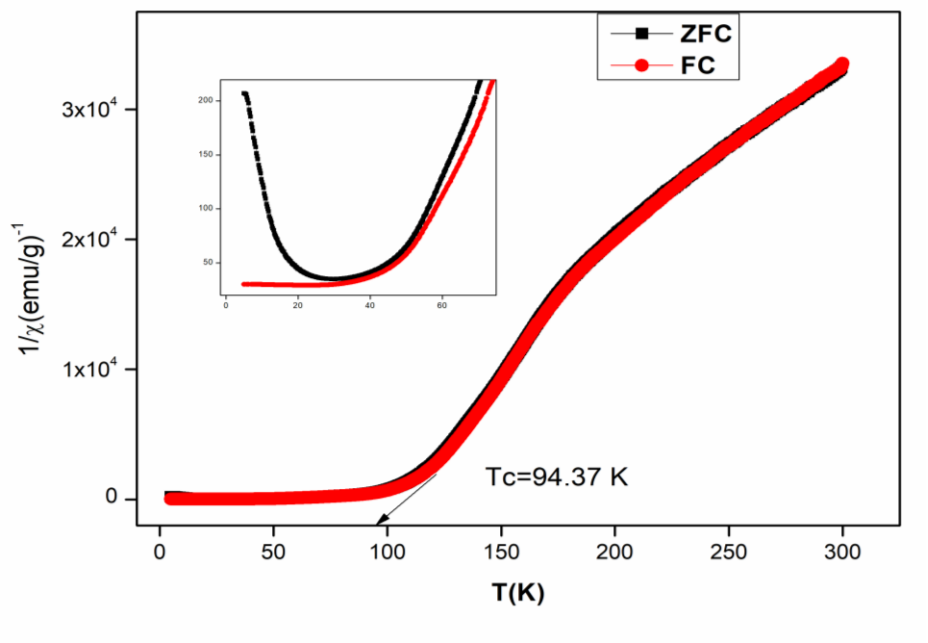

Fig. 3.8 Magnetic susceptibility as a function of temperature recorded at ± 2 T and applied magnetic field (H) at 100 Oe.

Figure 3.9 shows the polarization versus electric field (P-E) hysteresis curve of CCTMO ceramic measured at different temperatures and frequency of 150 Hz. It is observed from figure that loop shape changes in slimmer with increase of temperature, indicates the evolution process to relaxor ferroelectrics. The coercivity value obtained from the P-E hysteresis curve are 2.54, 2.23, 1.641 and 0.806 kV/cm, respectively, at 303 K, 323 K, 343 K and 364 K, respectively that explain the Value of Hc decreases with increasing temperature. The measured values of remnants polarizations for CCTMO ceramic are 0.259, 0.275, 0.317, and 0.364 $\mu C/cm^{-2}$, respectively at the same temperatures. The absence of saturation polarization is described by the combined effect of capacitor and resistor joint in parallel (loosy capacitor) [32].

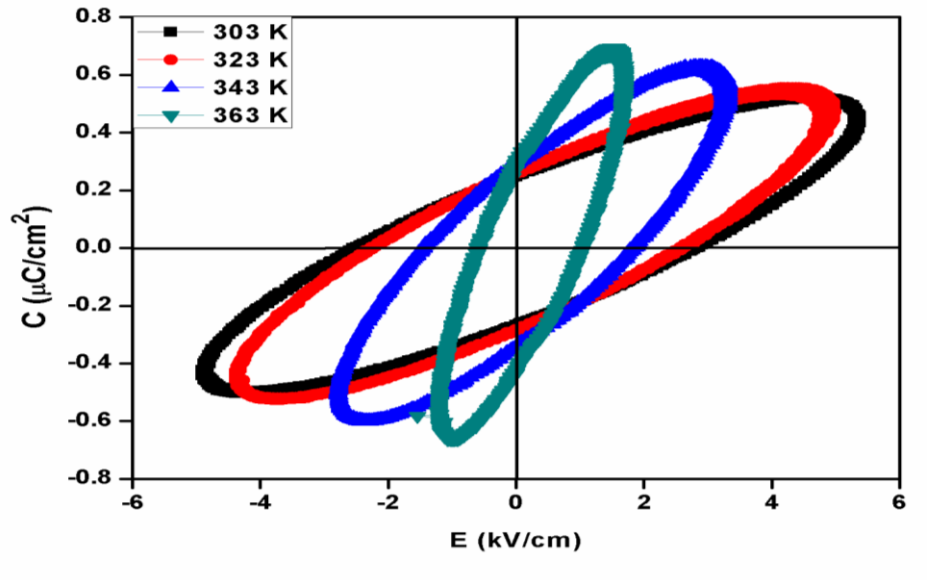

Fig. 3.9 P-E hysteresis loop for $CaCu_3TiMnO_{12}$ sintered at 1223 K for 8 h.

3.4 Conclusions

In this summary, manganese doped calcium copper titanium oxide; $CaCu_3Ti_3MnO_{12}$ (CCTMO) was successfully synthesized by using semi-wet route. Single phase formation of CCMTO ceramic was confirmed by XRD and average crystallite size obtained from the XRD results was found to be 34.77 ± 10 nm, which is close to the particle size (43.76 ± 10 nm) determined by TEM. The average grain size of sintered materials observed by SEM analysis was1.46 μm. EDX spectra confirmed that the presence of Ca, Cu, Ti, Mn, O element in CCTMO ceramic in stochiometric ratio as molecular formula. The value of dielectric constant (ε_r) and dielectric loss (tan δ) were found to be 100 and 0.1, respectively at 303 K and 100 Hz. Magnetic studies emphasized ferromagnetic behaviour at lower temperature and attain paramagnetic in nature at higher temperature.

[1] Deschanvres, A., Raveau, B., Tollemer, F. (1967) Substitution of copper for a divalent metal in perovskite-type titanates. *Bull. Soc. Chim. Fr*. **11**, 4077-78.

[2] Popielarz, R., Chiang, C. K., Nozaki, R., Obrzut, J. (2001). Dielectric properties of polymer/ferroelectric ceramic composites from 100 Hz to 10 GHz. *ACS Micro Lett.* **34**, 5910-5915.

[3] Li, J., Subramanian, M.A., Rosenfeld, H.D., Jones, C.Y., Toby, B.H., Sleight, A.W. (2004). Clues to the giant dielectric constant of $CaCu_3Ti_4O_{12}$ in the defect structure of $SrCu_3Ti_4O_{12}$. *Chem. Mater.* **16**(25), 5223-5225.

[4] Ramirez, A.P., Subramanian, M.A., Gardel, M., Blumberg, G., Li, D; Vogt, T., Shapiro, S.M.: Giant dielectric constant response in a copper-titanate. *Solid State Commun*. **115**(5), 217-220 (2000)

[5] Huang, Y., Shi, D., Li, Y., Li, G., Wang, Q., Liu, L., Fang, L. (2013) Effect of holding time on the dielectric properties and non-ohmic behaviour of $CaCu_3Ti_4O_{12}$ capacitor-varistors. *J Mater Sci-Mater EL*. **24**(6), 1994-1999.

[6] Ouyang, X., Habib, M., Cao, P., Wei, S., Huang, Z., Zhang, W., Gao, W. (2015). Enhanced extrinsic dielectric response of TiO2 modified $CaCu_3Ti_4O_{12}$ceramics. *Ceram. Int.* **41**(10), 13447-13454.

[7] Shay, D.P., Podraza, N.J., Donnelly, N.J., Randall, C.A. (2012). High energy density, high temperature capacitors utilizing Mn-doped $0.8CaTiO_3$–$0.2CaHfO_3$ ceramics. *J. Am. Ceram. Soc*. **95**(4), 1348-1355.

[8] West, D.L., Payne, D.A. (2003). Microstructure Development in Reactive-Templated Grain Growth of $Bi_{1/2}Na_{1/2}TiO_3$-Based Ceramics: Template and Formulation Effects. *J. Am. Ceram. Soc*. **86**(5), 769-774.

[9] Subramanian, M.A., Li, D., Duan, N., Reisner, B.A., Sleight, A.W. (2000). High dielectric constant in $ACu_3Ti_4O_{12}$ and $ACu_3Ti_3FeO_{12}$ phases. *J. Solid. State. Chem.* **151**(2), 323-325.

[10] Singh, L., Sin, B.C., Kim, I.W., Mandal, K.D., Chung. H, Lee., Y.A. (2016). A novel one-step flame synthesis method for tungsten-doped CCTO. *J. Am. Ceram Soc.* **99**(1), 27-34.

[11] Li, M., Feteira, A., Sinclair, D.C., West, A.R. (2000). Influence of Mn doping on the semiconducting properties of $CaCu_3Ti_4O_{12}$ ceramics. *Appl. Phys. let*. **88**(23), 232903.

[12] Adams, T.B., Sinclair, D.C., West, A.R. (2006). Characterization of grain boundary impedances in fine-and coarse-grained $CaC_{u3}T_{i4}O_{12}$ *Ceramics. Phys. Rev.* B. **73**(9), 094124.

[13] Sinclair, D.C., Adams, T.B., Morrison, F.D., West; A.R. (2000). $CaCu_3Ti_4O_{12}$ one-step internal barrier layer capacitor. *Appl. Phys. Lett.* **80**(12), 2153-2155.

[14] Li, W., Schwartz, R.W. (2006). ac conductivity relaxation processes in $CaCu_3Ti_4O_{12}$ ceramics: Grain boundary and domain boundary effects. *Appl. Phys. Lett.* **89**(24), 242906.

[15] Wu, L., Y, Zhu., S, Par., S, Shapiro., G, Shirane., J, Tafto. (2005). Defect structure of the high-dielectric-constant perovskite $CaCu_3Ti_4O_{12}$. *Phys. Rev. B.* **71**(1), 014118.

[16] Xu, D., He, K., Yu, R., Sun, X., Yang, Y., Xu, H., Yuan, H., Ma, J. (2015). High dielectric permittivity and low dielectric loss in sol–gel derived Zn doped $CaCu_3Ti_4O_{12}$ thin films. *Mater. Chem. Phys*. **153**, 229-35.

[17] Cho, A., Han, CS., Kang, M., Choi, W., Lee, J., Jeon. J., Yu, S., Jung, Y.S., Cho, Y.S. (2018). Direct Correlations of Grain Boundary Potentials to Chemical States and Dielectric Properties of Doped $CaCu_3Ti_4O_{12}$ Thin Films. *ACS appl. Mater. Inter.* **10**(18), 16203-16209.

[18] Chung, SY., Kim, ID., Kang SJ. (2004). Strong nonlinear current–voltage behaviour in perovskite-derivative calcium copper titanate. *Nat mater.* **3**(11), 774.

[19] Fang, T.T., Shiau, H. K. (2004). Mechanism for developing the boundary barrier layers of $CaCu_3Ti_4O_{12}$. *J. Am. Ceram. Soc.* **87**(11) 2072-9.

[20] Kim, C. H., Jang, Y. H., Seo, S. J., Song, C. H., Son, J. Y., Yang, Y. S., & Cho, J. H. (2012). Effect of Mn doping on the temperature-dependent anomalous giant dielectric behaviour of $CaCu_3Ti_4O_{12}$. *Phys. Rev. B.* **85**(24) 245210.

[21] Thongbai, P., Pinitsoontorn, S., Amornkitbamrung, V., Yamwong, T., Maensiri, S., Chindaprasirt, P. (2013): Reducing loss tangent by controlling microstructure and electrical responses in $CaCu_3Ti_4O_{12}$ ceramics prepared by a simple combustion method. *Int. J. Appl. Ceram. Tec*. **10**, E77-E87.

[22] Lin, Y. H., Cai, J., Li, M., Nan, C. W., He, J. (2006). High dielectric and nonlinear electrical behaviors in TiO_2 -rich Ca $Cu_3Ti_4O_{12}$ ceramics. *Appl. Phys. Lett.* **88**(17), 172902.

[23] Khare, A., Yadava, S. S., Mandal, K. D., Mukhopadhyay, N. K. (2016). Effect of sintering duration on the dielectric properties of $0.9BaTiO_3$–$0.1CaCu_3Ti_4O_{12}$ nanocomposite synthesized by solid state route. *Microelectron. Eng.* 164:1-6.

[24] Kim, H.E., Choi, S.M., Hong, Y. W. (2014). Improved dielectric properties of the $CaCu_3Ti_4O_{12}$ composites using $BaTiO_3$-coated powder as precursor. *J. Alloys Compd.* **610**, 594-599.

[25] Gautam, P., Khare, A., Sharma, S., Singh, N. B., Mandal, K. D. (2016). Characterization of $Bi_{2/3}Cu_3Ti_4O_{12}$ ceramics synthesized by semi-wet route. *Pro Nat Sci-Mater.* **26**(6), 567-571.

[26] George, M., Nair, S. S., Malini, K. A., Joy, P. A., Anantharaman, M. R. (2007). Finite size effects on the electrical properties of sol–gel synthesized $CoFe_2O_4$ powders: deviation from Maxwell–Wagner theory and evidence of surface polarization effects. *J Phys D: Appl Phys.* **40**(6), 1593.

[27] Jia, R., Zhao, X., Li, J., Tang, X. (2014). Colossal breakdown electric field and dielectric response of Al-doped $CaCu_3Ti_4O_{12}$ ceramics. *Mater. Sci. Eng. B*, **185**, 79-85.

[28] Sun, D.L; Wu, A.Y; Yin, S.T. (2008). Structure, properties, and impedance spectroscopy of $CaCu_3Ti_4O_{12}$ ceramics prepared by sol–gel process. *J. Am. Ceram. Soc.* **91**(1), 169-73.

[29] Wu, X., Huang, K., Yuan, L., Feng, S. (2018). Fabrication of ultralong perovskite structure nanotubes. *RSC Adv*. **8**(1), 367-373.

[30] Mo, Z.J., Shen, J., Gao, X. Q., Liu, Y., Wu, J. F., Shen, B. G., Sun, J. R. (2015). Magnetic properties and magnetocaloric effects in HoPd intermetallic. *Chinese. Phys B.* **24**(3), 037503.

[31] Han, D., Wu, Z., Wang, Z., Yang, S. (2012). Oriented Mn-doped CuO nanowire arrays. *Nanotechnology.* **27**(13), 135603.

[32] Yadava, S. S., Singh, L., Sharma, S., Mandal, K. D., Singh, N. B. (2016). Effect of temperature on the dielectric and ferroelectric properties of a nanocrystalline hexagonal $Ba_4YMn_3O_{11.5-\delta}$ ceramic synthesized by a chemical route. *RSC Adv.* **6**(72), 68247-68253.